

Observation of $D^0 - \bar{D}^0$ Mixing in e^+e^- Collisions

B. R. Ko,²⁷ E. Won,²⁷ I. Adachi,¹² H. Aihara,⁶¹ K. Arinstein,⁴ D. M. Asner,⁴⁶ V. Aulchenko,⁴ T. Aushev,²¹ A. Bala,⁴⁷ V. Bhardwaj,³⁷ B. Bhuyan,¹⁵ A. Bobrov,⁴ A. Bondar,⁴ A. Bozek,⁴¹ M. Bračko,^{31,22} T. E. Browder,¹¹ D. Červenkov,⁵ A. Chen,³⁸ B. G. Cheon,¹⁰ K. Chilikin,²¹ R. Chistov,²¹ I.-S. Cho,⁶⁸ K. Cho,²⁶ V. Chobanova,³² S.-K. Choi,⁹ Y. Choi,⁵⁴ D. Cinabro,⁶⁷ J. Dalseno,^{32,57} M. Danilov,^{21,34} Z. Doležal,⁵ Z. Drásal,⁵ D. Dutta,¹⁵ K. Dutta,¹⁵ S. Eidelman,⁴ D. Epifanov,⁶¹ H. Farhat,⁶⁷ J. E. Fast,⁴⁶ T. Ferber,⁷ V. Gaur,⁵⁶ S. Ganguly,⁶⁷ A. Garmash,⁴ R. Gillard,⁶⁷ R. Glattauer,¹⁸ Y. M. Goh,¹⁰ B. Golob,^{30,22} J. Haba,¹² T. Hara,¹² H. Hayashii,³⁷ X. H. He,⁴⁸ T. Higuchi,²⁵ Y. Hoshi,⁵⁹ W.-S. Hou,⁴⁰ H. J. Hyun,²⁸ T. Iijima,^{36,35} A. Ishikawa,⁶⁰ R. Itoh,¹² Y. Iwasaki,¹² T. Iwashita,²⁵ I. Jaegle,¹¹ T. Julius,³³ T. Kawasaki,⁴³ C. Kiesling,³² D. Y. Kim,⁵³ J. B. Kim,²⁷ J. H. Kim,²⁶ M. J. Kim,²⁸ Y. J. Kim,²⁶ J. Klucar,²² P. Kodyš,⁵ S. Korpar,^{31,22} P. Križan,^{30,22} P. Krokovny,⁴ T. Kuhr,²⁴ T. Kumita,⁶³ A. Kuzmin,⁴ Y.-J. Kwon,⁶⁸ J. S. Lange,⁸ S.-H. Lee,²⁷ J. Li,⁵² Y. Li,⁶⁶ J. Libby,¹⁶ C. Liu,⁵¹ Z. Q. Liu,¹⁷ P. Lukin,⁴ D. Matvienko,⁴ K. Miyabayashi,³⁷ H. Miyata,⁴³ G. B. Mohanty,⁵⁶ A. Moll,^{32,57} R. Mussa,²⁰ Y. Nagasaka,¹³ E. Nakano,⁴⁵ M. Nakao,¹² Z. Natkaniec,⁴¹ M. Nayak,¹⁶ E. Nedelkovska,³² N. K. Nisar,⁵⁶ O. Nitoh,⁶⁴ S. Ogawa,⁵⁸ S. Okuno,²³ G. Pakhlova,²¹ C. W. Park,⁵⁴ H. K. Park,²⁸ T. K. Pedlar,⁶⁹ T. Peng,⁵¹ M. Petrič,²² L. E. Piilonen,⁶⁶ M. Ritter,³² M. Röhrken,²⁴ A. Rostomyan,⁷ S. Ryu,⁵² H. Sahoo,¹¹ Y. Sakai,¹² L. Santelj,²² T. Sanuki,⁶⁰ V. Savinov,⁴⁹ O. Schneider,²⁹ G. Schnell,^{1,14} C. Schwanda,¹⁸ A. J. Schwartz,⁶ R. Seidl,⁵⁰ O. Seon,³⁵ M. E. Sevier,³³ M. Shapkin,¹⁹ C. P. Shen,² T.-A. Shibata,⁶² J.-G. Shiu,⁴⁰ B. Shwartz,⁴ A. Sibidanov,⁵⁵ F. Simon,^{32,57} J. B. Singh,⁴⁷ Y.-S. Sohn,⁶⁸ A. Sokolov,¹⁹ S. Stanič,⁴⁴ M. Starič,²² M. Steder,⁷ T. Sumiyoshi,⁶³ U. Tamponi,^{20,65} G. Tatishvili,⁴⁶ Y. Teramoto,⁴⁵ K. Trabelsi,¹² M. Uchida,⁶² S. Uehara,¹² T. Uglov,^{21,70} Y. Unno,¹⁰ S. Uno,¹² P. Urquijo,³ Y. Usov,⁴ S. E. Vahsen,¹¹ C. Van Hulse,¹ P. Vanhoefer,³² G. Varner,¹¹ A. Vinokurova,⁴ V. Vorobyev,⁴ M. N. Wagner,⁸ C. H. Wang,³⁹ M.-Z. Wang,⁴⁰ P. Wang,¹⁷ Y. Watanabe,²³ H. Yamamoto,⁶⁰ Y. Yamashita,⁴² S. Yashchenko,⁷ Y. Yook,⁶⁸ C. C. Zhang,¹⁷ Z. P. Zhang,⁵¹ V. Zhilich,⁴ and A. Zupanc²⁴

(The Belle Collaboration)

¹University of the Basque Country UPV/EHU, 48080 Bilbao

²Beihang University, Beijing 100191

³University of Bonn, 53115 Bonn

⁴Budker Institute of Nuclear Physics SB RAS and Novosibirsk State University, Novosibirsk 630090

⁵Faculty of Mathematics and Physics, Charles University, 121 16 Prague

⁶University of Cincinnati, Cincinnati, Ohio 45221

⁷Deutsches Elektronen-Synchrotron, 22607 Hamburg

⁸Justus-Liebig-Universität Gießen, 35392 Gießen

⁹Gyeongang National University, Chinju 660-701

¹⁰Hanyang University, Seoul 133-791

¹¹University of Hawaii, Honolulu, Hawaii 96822

¹²High Energy Accelerator Research Organization (KEK), Tsukuba 305-0801

¹³Hiroshima Institute of Technology, Hiroshima 731-5193

¹⁴IKERBASQUE, Basque Foundation for Science, 48011 Bilbao

¹⁵Indian Institute of Technology Guwahati, Assam 781039

¹⁶Indian Institute of Technology Madras, Chennai 600036

¹⁷Institute of High Energy Physics, Chinese Academy of Sciences, Beijing 100049

¹⁸Institute of High Energy Physics, Vienna 1050

¹⁹Institute for High Energy Physics, Protvino 142281

²⁰INFN - Sezione di Torino, 10125 Torino

²¹Institute for Theoretical and Experimental Physics, Moscow 117218

²²J. Stefan Institute, 1000 Ljubljana

²³Kanagawa University, Yokohama 221-8686

²⁴Institut für Experimentelle Kernphysik, Karlsruher Institut für Technologie, 76131 Karlsruhe

²⁵Kavli Institute for the Physics and Mathematics of the Universe (WPI), University of Tokyo, Kashiwa 277-8583

²⁶Korea Institute of Science and Technology Information, Daejeon 305-806

²⁷Korea University, Seoul 136-713

²⁸Kyungpook National University, Daegu 702-701

²⁹École Polytechnique Fédérale de Lausanne (EPFL), Lausanne 1015

³⁰Faculty of Mathematics and Physics, University of Ljubljana, 1000 Ljubljana

³¹University of Maribor, 2000 Maribor

³²Max-Planck-Institut für Physik, 80805 München

³³School of Physics, University of Melbourne, Victoria 3010

³⁴Moscow Physical Engineering Institute, Moscow 115409

- ³⁵Graduate School of Science, Nagoya University, Nagoya 464-8602
³⁶Kobayashi-Maskawa Institute, Nagoya University, Nagoya 464-8602
³⁷Nara Women's University, Nara 630-8506
³⁸National Central University, Chung-li 32054
³⁹National United University, Miao Li 36003
⁴⁰Department of Physics, National Taiwan University, Taipei 10617
⁴¹H. Niewodniczanski Institute of Nuclear Physics, Krakow 31-342
⁴²Nippon Dental University, Niigata 951-8580
⁴³Niigata University, Niigata 950-2181
⁴⁴University of Nova Gorica, 5000 Nova Gorica
⁴⁵Osaka City University, Osaka 558-8585
⁴⁶Pacific Northwest National Laboratory, Richland, Washington 99352
⁴⁷Panjab University, Chandigarh 160014
⁴⁸Peking University, Beijing 100871
⁴⁹University of Pittsburgh, Pittsburgh, Pennsylvania 15260
⁵⁰RIKEN BNL Research Center, Upton, New York 11973
⁵¹University of Science and Technology of China, Hefei 230026
⁵²Seoul National University, Seoul 151-742
⁵³Soongsil University, Seoul 156-743
⁵⁴Sungkyunkwan University, Suwon 440-746
⁵⁵School of Physics, University of Sydney, NSW 2006
⁵⁶Tata Institute of Fundamental Research, Mumbai 400005
⁵⁷Excellence Cluster Universe, Technische Universität München, 85748 Garching
⁵⁸Toho University, Funabashi 274-8510
⁵⁹Tohoku Gakuin University, Tagajo 985-8537
⁶⁰Tohoku University, Sendai 980-8578
⁶¹Department of Physics, University of Tokyo, Tokyo 113-0033
⁶²Tokyo Institute of Technology, Tokyo 152-8550
⁶³Tokyo Metropolitan University, Tokyo 192-0397
⁶⁴Tokyo University of Agriculture and Technology, Tokyo 184-8588
⁶⁵University of Torino, 10124 Torino
⁶⁶CNP, Virginia Polytechnic Institute and State University, Blacksburg, Virginia 24061
⁶⁷Wayne State University, Detroit, Michigan 48202
⁶⁸Yonsei University, Seoul 120-749
⁶⁹Luther College, Decorah, Iowa 52101
⁷⁰Moscow Institute of Physics and Technology, Moscow Region 141700

We observe $D^0 - \bar{D}^0$ mixing in the decay $D^0 \rightarrow K^+ \pi^-$ using a data sample of integrated luminosity 976 fb^{-1} collected with the Belle detector at the KEKB e^+e^- asymmetric-energy collider. We measure the mixing parameters $x'^2 = (0.09 \pm 0.22) \times 10^{-3}$ and $y' = (4.6 \pm 3.4) \times 10^{-3}$ and the ratio of doubly Cabibbo-suppressed to Cabibbo-favored decay rates $R_D = (3.53 \pm 0.13) \times 10^{-3}$, where the uncertainties are statistical and systematic combined. Our measurement excludes the no-mixing hypothesis at the 5.1 standard deviation level.

PACS numbers: 12.15.Ff, 13.25.Ft, 14.40.Lb

A weakly decaying flavored neutral meson is a two-state quantum system with an allowed transition between the two states. This transition is referred to as neutral meson mixing and originates from the difference between the flavor and mass eigenstates of the meson-antimeson system with a well-known rate depending on elements of the Cabibbo-Kobayashi-Maskawa matrix [1, 2]. Mixing phenomena are well established for K^0 , B^0 , and B_s^0 mesons and their mixing rates are consistent with predictions based on the standard model (SM) [3]. D^0 mixing has also recently been observed in hadron collider experiments [4, 5], confirming a previous $D^0 - \bar{D}^0$ mixing signal [6] based mainly on combined evidence from three different experiments [7–9].

The phenomenology of meson mixing is described by

two parameters, $x = \Delta m/\Gamma$ and $y = \Delta\Gamma/2\Gamma$, where Δm and $\Delta\Gamma$ are the mass and width differences between the two mass eigenstates and Γ is the average decay width of the mass eigenstates. While the finite mixing parameters of the K^0 , B^0 , and B_s^0 mesons are well measured, those for the D^0 meson are not [6]. The mixing parameters x and y are difficult to calculate [10, 11], which complicates the interpretation of experimental measurements against the SM. Nevertheless, it is still of great interest to improve the measurement of the D^0 mixing parameters to search for possible beyond-SM physics contributions [12]. It is also very valuable to confirm D^0 mixing in e^+e^- collisions and provide further independent determinations of the D^0 mixing parameters where the experimental conditions are quite different from those in hadron collider

experiments.

In this Letter, we report the first observation of $D^0 - \bar{D}^0$ mixing from an e^+e^- collision experiment by measuring the time-dependent ratio of the $D^0 \rightarrow K^+\pi^-$ to $D^0 \rightarrow K^-\pi^+$ decay rates. The consideration of charge-conjugated decays is implied throughout this Letter. We refer to $D^0 \rightarrow K^+\pi^-$ as wrong-sign (WS) and $D^0 \rightarrow K^-\pi^+$ as right-sign (RS) decays. We tag the RS and WS decays through the decay chain $D^{*+} \rightarrow D^0(\rightarrow K^\mp\pi^\pm)\pi_s^+$ by comparing the charge of the π from the D^0 decay and the charge of the low-momentum π_s from the D^{*+} decay. The RS decay amplitude is the sum of the amplitudes for Cabibbo-favored (CF) decay $D^0 \rightarrow K^-\pi^+$ and $D^0 - \bar{D}^0$ mixing followed by the doubly-Cabibbo-suppressed (DCS) decay $\bar{D}^0 \rightarrow K^-\pi^+$, where the latter is very small compared to the former and is therefore neglected. In contrast, the WS decay amplitude is the sum of two comparable decay amplitudes for the DCS decay $D^0 \rightarrow K^+\pi^-$ and $D^0 - \bar{D}^0$ mixing followed by the CF decay $\bar{D}^0 \rightarrow K^+\pi^-$. Assuming charge-conjugation and parity (CP) conservation and that the mixing parameters are small ($|x| \ll 1$ and $|y| \ll 1$), the time-dependent RS and WS decay rates are

$$\begin{aligned}\Gamma_{\text{RS}}(\tilde{t}/\tau) &\approx |\mathcal{A}_{\text{CF}}|^2 e^{-\frac{\tilde{t}}{\tau}}, \\ \Gamma_{\text{WS}}(\tilde{t}/\tau) &\approx |\mathcal{A}_{\text{CF}}|^2 e^{-\frac{\tilde{t}}{\tau}} \\ &\times \left(R_D + \sqrt{R_D} y' \frac{\tilde{t}}{\tau} + \frac{x'^2 + y'^2}{4} \left(\frac{\tilde{t}}{\tau} \right)^2 \right) \quad (1)\end{aligned}$$

to second order in the mixing parameters. In Eq. (1), \tilde{t} is the true proper decay time, \mathcal{A}_{CF} is the CF decay amplitude, τ is the D^0 lifetime, R_D is the ratio of DCS to CF decay rates, $x' = x \cos \delta + y \sin \delta$, and $y' = y \cos \delta - x \sin \delta$, where δ is the strong phase difference between the DCS and CF decay amplitudes. The time-dependent ratio of WS to RS decay rates is then

$$R(\tilde{t}/\tau) = \frac{\Gamma_{\text{WS}}(\tilde{t}/\tau)}{\Gamma_{\text{RS}}(\tilde{t}/\tau)} \approx R_D + \sqrt{R_D} y' \frac{\tilde{t}}{\tau} + \frac{x'^2 + y'^2}{4} \left(\frac{\tilde{t}}{\tau} \right)^2, \quad (2)$$

which is a quadratic function of \tilde{t}/τ .

In order to measure the mixing parameters using Eq. (2), the measured proper decay time should be approximately the true proper decay time. This condition is satisfied in hadron collider experiments [4, 5] where the tagged D 's have a decay time much larger than the resolution on \tilde{t} . At a B -factory, however, the mean decay time of the tagged D 's, shown in Fig. 2, is approximately the D^0 lifetime, which is comparable to the resolution on \tilde{t} ; thus, the resolution effect must be taken into account. Our approach here is to measure the time-dependent ratio of WS to RS decays, given by

$$R(t/\tau) = \frac{\int_{-\infty}^{+\infty} \Gamma_{\text{WS}}(\tilde{t}/\tau) \mathcal{R}(t/\tau - \tilde{t}/\tau) d(\tilde{t}/\tau)}{\int_{-\infty}^{+\infty} \Gamma_{\text{RS}}(\tilde{t}/\tau) \mathcal{R}(t/\tau - \tilde{t}/\tau) d(\tilde{t}/\tau)}, \quad (3)$$

where t is the reconstructed proper decay time and $\mathcal{R}(t/\tau - \tilde{t}/\tau)$ is the resolution function of the real decay time, \tilde{t} .

The data used in this analysis are recorded at the $\Upsilon(nS)$ resonances ($n = 1, 2, 3, 4, 5$) or near the $\Upsilon(4S)$ resonance with the Belle detector at the e^+e^- asymmetric-energy collider KEKB [13]. The data sample corresponds to an integrated luminosity of 976 fb^{-1} . The Belle detector is a large-solid-angle magnetic spectrometer that consists of a silicon vertex detector (SVD), a 50-layer central drift chamber (CDC), an array of aerogel threshold Cherenkov counters (ACC), a barrel-like arrangement of time-of-flight scintillation counters (TOF), and an electromagnetic calorimeter comprising CsI(Tl) crystals (ECL) located inside a superconducting solenoid coil that provides a 1.5 T magnetic field. An iron flux return located outside the coil is instrumented to detect K_L^0 mesons and identify muons. A detailed description of the Belle detector can be found in Ref. [14].

We require that charged tracks originate from the e^+e^- interaction point (IP) with an impact parameter less than 4 cm in the beam direction (the z axis) and 2 cm in the transverse plane and have a transverse momentum greater than $0.1 \text{ GeV}/c$. All charged tracks are required to have at least two associated hits each in the z and azimuthal strips of the SVD to assure good spatial resolution of the decay vertices of D^0 mesons. Charged tracks are identified as K or π candidates using the ratio of particle identification likelihoods, $\mathcal{P}_{K\pi} \equiv \mathcal{L}_K/(\mathcal{L}_K + \mathcal{L}_\pi)$, reconstructed from the track-associated data in the CDC, TOF, and ACC. We require $\mathcal{P}_{K\pi} > 0.4$ for K , $\mathcal{P}_{K\pi} < 0.7$ for π and $\mathcal{P}_{K\pi} < 0.9$ for π_s candidates. The efficiency and K/π misidentification rate of the K selection are 91% and 12% and those of the π selection are 94% and 18%. We also apply a loose electron veto criterion using the ECL information for all charged tracks. Oppositely-charged K and π candidates are combined to form a D^0 candidate by fitting them to a common vertex; the resulting D^0 candidate is fit to the IP to give the D^{*+} vertex. A D^{*+} candidate is reconstructed by combining a D^0 candidate—a $K\pi$ combination with invariant mass within $\pm 20 \text{ MeV}/c^2$ (i.e., $\sim \pm 3\sigma$) of the nominal D^0 mass [3]—with a π_s . The π_s is further constrained to pass through the D^{*+} vertex. The sum of the reduced χ^2 of the D^{*+} vertex fit and π_s fit to the D^{*+} vertex is required to be less than 16.

There is a significant contribution to the WS sample from RS decays where both K and π candidates are misidentified as π and K , respectively. We remove these with tighter particle identification requirements, $\mathcal{P}_{K\pi} > 0.99$ for K and $\mathcal{P}_{K\pi} < 0.01$ for π , if $M(K\pi)_{\text{swap}}$, the invariant mass of the $K\pi$ combination when swapping the nominal mass of K and π track candidates, is within $\pm 25 \text{ MeV}/c^2$ of the nominal D^0 mass. To remove combinatorial background due to random unassociated charged track combinations that meet all the other requirements,

we require the D^{*+} meson momentum calculated in the center-of-mass system to be greater than 2.5, 2.6, and 3.0 GeV/c for the data taken below the $\Upsilon(4S)$, at the $\Upsilon(4S)$, and above the $\Upsilon(4S)$ resonance, respectively. This momentum requirement also removes $D^{*+} \rightarrow D^0 \pi_s^+$ decays from B meson decays, which do not give the proper decay time of the D^0 meson due to the finite B -meson lifetime.

The selection criteria described above are chosen by maximizing $R_{\text{WS}} \mathcal{N}_{\text{S}}^{\text{RS}} / \sqrt{R_{\text{WS}} \mathcal{N}_{\text{S}}^{\text{RS}} + \mathcal{N}_{\text{B}}^{\text{WS}}}$, where R_{WS} is the nominal ratio of WS to RS decay rates [3], $\mathcal{N}_{\text{S}}^{\text{RS}}$ is the number of events in the RS signal region of the $D^{*+}-D^0$ mass difference, $\Delta M \equiv M(D^{*+} \rightarrow D^0(\rightarrow K\pi)\pi_s^+) - M(D^0 \rightarrow K\pi)$, and $\mathcal{N}_{\text{B}}^{\text{WS}}$ is that in the WS sideband regions of ΔM . We define the signal region as $\Delta M \in [0.144, 0.147]$ GeV/c² and the background sidebands as $\Delta M \in [0.141, 0.142]$ or $[0.149, 0.151]$ GeV/c². When counting $\mathcal{N}_{\text{S}}^{\text{RS}}$, we subtract background candidates in the signal region using candidates in the RS sideband regions.

The measured D^0 proper decay time is calculated as $t = m_{D^0} \vec{L} \cdot \vec{p} / |\vec{p}|^2$ where \vec{L} is the vector joining the decay and production vertices of the D^0 , \vec{p} is the D^0 momentum, and m_{D^0} and τ are the nominal D^0 mass and lifetime [3]. We require the uncertainty on t to satisfy $\sigma_t/\tau < 1.0$, and $t/\tau \in [-5, 10]$. These selections are determined from 5000 simplified simulated experiments by maximizing our sensitivity to the mixing parameters and minimizing the systematic biases in them.

Using these selections, we find no significant backgrounds in WS candidates that peak in the signal region from a large-statistics sample of fully simulated $e^+e^- \rightarrow$ hadrons events in our GEANT3-based [15] Monte Carlo (MC) simulation. Figure 1 shows the time-integrated distributions of ΔM from RS and WS candidate events after applying all the selections described above.

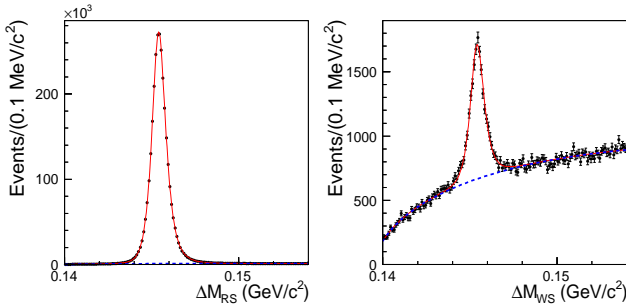


FIG. 1: Time-integrated distributions for the mass difference of RS (left) and WS (right) candidates. Points with error bars are the data; full and dashed lines are, respectively, the signal and background fits described in the text.

The time-integrated RS signal shown in Fig. 1 is parametrized as a sum of Gaussian and Johnson S_U [16] distributions with a common mean. The time-dependent RS signal in each bin of the proper decay time is fit

with a Johnson S_U only. The shapes of the WS signal are fixed using the corresponding RS signal shapes, and fit with only the signal normalization allowed to vary. The backgrounds in RS and WS decay events are fit independently and are parametrized with the form $(\Delta M - m_{\pi^+})^\alpha e^{-\beta(\Delta M - m_{\pi^+})}$, where α and β are free fit parameters, and m_{π^+} is the nominal mass of π^+ [3]. The fits give $2\,980\,710 \pm 1885$ RS and $11\,478 \pm 177$ WS decays, giving an inclusive ratio of WS to RS decay rates of $(3.851 \pm 0.059) \times 10^{-3}$. The uncertainty is statistical only.

We obtain the resolution function of Eq. (3) from the proper decay time distribution of RS decays after subtracting a small level of background events using the sideband regions defined above. This is shown in Fig. 2. We parametrize the proper decay time distribution of RS

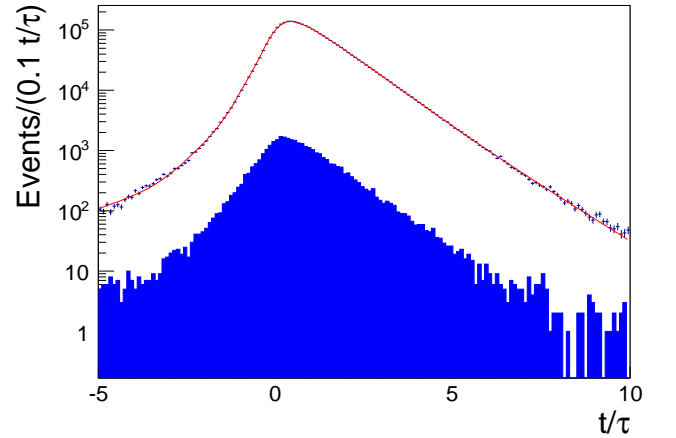


FIG. 2: Distribution of the proper decay time from background-subtracted RS decays in the signal region (points with error bars) and in the sideband regions (shaded). The curve shows the fit to the signal.

decays with the convolution of an exponential and a resolution function that is constructed as the sum of four Gaussians, $\mathcal{R}(t/\tau) = \sum_{i=1}^4 f_i G_i(t/\tau; \mu_i, \sigma_i)$, where G_i is a Gaussian distribution with mean μ_i and width σ_i and f_i is its weight. The mean μ_i is further parametrized with $\mu_i = \mu_1 + a\sigma_i$, where μ_1 is the mean of the core Gaussian G_1 ($i = 2, 3, 4$). The parameters a and μ_1 describe a possible asymmetry of the resolution function. All parameters of the resolution function float freely and the fit is shown in Fig. 2. The D^0 lifetime is also a free fit parameter, for which we obtain (408.5 ± 0.9) fs, where the uncertainty is statistical only. This D^0 lifetime is consistent with the world-average value [3] and the other Belle measurement [17], which gives further confidence in our parametrization of the resolution function.

To calculate the time-dependent WS to RS decay rate ratio, we divide the samples shown in Fig. 1 into ten bins of proper decay time. Our binning choice is made us-

ing 5000 simplified simulated experiments to maximize the sensitivity to the mixing parameters. Figure 3 shows the time-dependent ratios of WS to RS decay rates. The

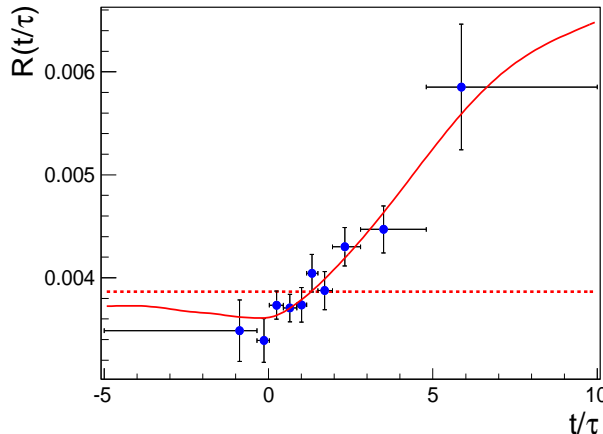


FIG. 3: The time-dependent ratios of WS to RS decay rates. Points with error bars reflect the data and their total uncertainties. The lines show the fit with (solid) and without (dashed) the mixing hypothesis.

average value of the proper decay time in each bin is determined with the parametrization for the reconstructed RS proper decay time distribution shown in Fig. 2.

Prior to our fit to the time-dependent ratios of WS to RS decay rates, we estimate possible systematic effects. We validate the analysis procedure with the fully simulated MC events with several different input values of the mixing parameters and find results consistent with the input parameters. The dominant sources of systematic uncertainties are from fitting the ΔM distributions and uncertainties on the resolution function that do not cancel out in Eq. (3). However, these are estimated to be less than a tenth of the statistical uncertainty, which is estimated in simulated simplified experiments. Other sources of uncertainty are the binning of the proper decay time and the reconstruction efficiencies of WS and RS decays. These effects should cancel in the WS to RS ratio measurement. We estimate these with simulated simplified experiments and, indeed, find a negligible contribution of $< \mathcal{O}(10^{-4})$ on the mixing parameters and so ignore them. The systematic uncertainties due to fitting the ΔM distributions are estimated in the bins of the proper decay time and are added to the statistical uncertainties of the bin in quadrature, albeit with negligible effect.

Our fits to the time-dependent ratios of WS to RS decays using Eq. (3) are shown in Fig. 3. We test two hypotheses, with and without mixing, and the results are listed in Table I. The mixing parameters measured in this analysis agree with previous results from both hadron collider experiments [5, 18] using a similar method, as well as

TABLE I: Results of the time-dependent fit to $R(t/\tau)$, where DOF stands for the degrees of freedom. The uncertainties are statistical and systematic combined.

Test hypothesis	Parameters	Fit results		Correlation coefficient	
(χ^2/DOF)		(10^{-3})	R_D	y'	x'^2
Mixing (4.2/7)	R_D	3.53 ± 0.13	1	-0.865	+0.737
	y'	4.6 ± 3.4		1	-0.948
	x'^2	0.09 ± 0.22			1
No Mixing (33.5/9)	R_D	3.864 ± 0.059			

with the results of alternate experimental methods from e^+e^- collision experiments [7, 19] and are summarized in Table II.

TABLE II: Measured $D^0 - \bar{D}^0$ mixing parameters in $D^0 \rightarrow K^+\pi^-$ decays from this work and others, where we display the total uncertainty. All measurements assume CP conservation.

Experiment	$R_D (\times 10^{-3})$	$y' (\times 10^{-3})$	$x'^2 (\times 10^{-3})$
Belle [19]	3.64 ± 0.17	$0.6^{+4.0}_{-3.9}$	$0.18^{+0.21}_{-0.23}$
BaBar [7]	3.03 ± 0.19	9.7 ± 5.4	-0.22 ± 0.37
CDF [5]	3.51 ± 0.35	4.3 ± 4.3	0.08 ± 0.18
LHCb [18]	3.568 ± 0.066	4.8 ± 1.0	0.055 ± 0.049
Belle (this work)	3.53 ± 0.13	4.6 ± 3.4	0.09 ± 0.22

As a check of our results in Table I, we repeat the analysis in two independent sub-samples. One corresponds to an integrated luminosity of 400 fb^{-1} (the “old sample”) that is used in our previous publication [19] with a different method than used here. The other is the rest of our full data sample, corresponding to an integrated luminosity of 576 fb^{-1} (the “new sample”). These two independent sub-samples are fed through this analysis separately. The results from the old and new samples (with statistical uncertainty only) are $(R_D, y', x'^2) = (3.65 \pm 0.22, -0.2 \pm 5.4, 0.36 \pm 0.32) \times 10^{-3}$ and $(3.45 \pm 0.17, 7.6 \pm 4.4, -0.09 \pm 0.30) \times 10^{-3}$, respectively, which are compatible with the results from the full data sample. Furthermore, the results of this analysis using the old sample are consistent with our previous publication [19], which is superseded by the results of this analysis.

The χ^2 difference between the “no-mixing” and “mixing” hypotheses, $\Delta\chi^2 = \chi^2_{\text{no-mixing}} - \chi^2_{\text{mixing}}$, is 29.3 for two degrees of freedom, corresponding to a probability of 4.3×10^{-7} ; this implies the no-mixing hypothesis is excluded at the 5.1 standard deviation level. Thus, we observe $D^0 - \bar{D}^0$ mixing for the first time in an e^+e^- collision experiment. We also show this in Fig. 4 with the 1σ , 3σ , and 5σ contours around the best fit point in the (x'^2, y') plane.

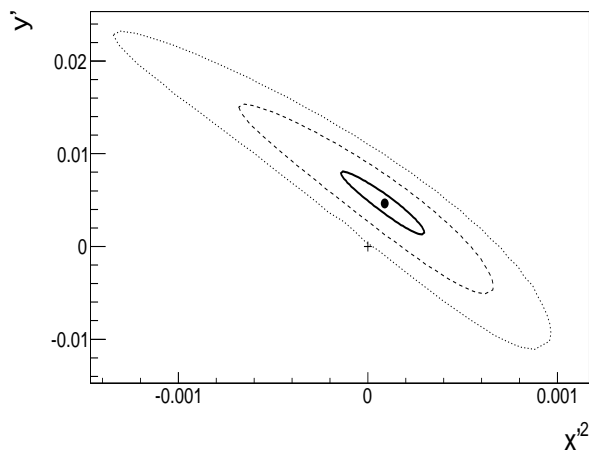


FIG. 4: Best-fit point and contours in the (x'^2, y') plane. The solid, dashed, and dotted lines, respectively, correspond to 1, 3, and 5 standard Gaussian deviations from the best fit. The cross is the no-mixing point.

In summary, we report the first observation of $D^0 - \bar{D}^0$ mixing in e^+e^- collisions by measuring the time-dependent ratios of the WS to RS decay rates, providing $x'^2 = (0.09 \pm 0.22) \times 10^{-3}$, $y' = (4.6 \pm 3.4) \times 10^{-3}$, and $R_D = (3.53 \pm 0.13) \times 10^{-3}$. Our results agree well with those from hadron collider experiments [5, 18] performed in very different experimental conditions.

We thank the KEKB group for excellent operation of the accelerator; the KEK cryogenics group for efficient solenoid operations; and the KEK computer group, the NII, and PNNL/EMSL for valuable computing and SINET4 network support. We acknowledge support from MEXT, JSPS and Nagoya's TLPRC (Japan); ARC and DIISR (Australia); FWF (Austria); NSFC (China); MSMT (Czechia); CZF, DFG, and VS (Germany); DST (India); INFN (Italy); MOE, MSIP, NRF, GSDC of KISTI, BK21Plus, and WCU (Korea); MNiSW and NCN (Poland); MES and RFAAE (Russia); ARRS (Slovenia); IKERBASQUE and UPV/EHU (Spain); SNSF (Switzerland); NSC and MOE (Taiwan); and DOE and NSF (USA). B. R. Ko acknowledges support by NRF Grant No. 2010-0021279, and E. Won by NRF Grant No. 2010-

0021174.

-
- [1] N. Cabibbo, Phys. Rev. Lett. **10**, 531 (1963).
 - [2] M. Kobayashi and T. Maskawa, Prog. Theor. Phys., **49**, 652 (1973).
 - [3] J. Beringer *et al.* (Particle Data Group), Phys. Rev. D **86**, 010001 (2012).
 - [4] R. Aaij *et al.* (LHCb collaboration), Phys. Rev. Lett. **110**, 101802 (2013).
 - [5] T. Aaltonen *et al.* (CDF collaboration), Phys. Rev. Lett. **111**, 231802 (2013).
 - [6] Y. Amhis *et al.* (Heavy Flavor Averaging Group), [arXiv:1207.1158v2\[hep-ex\]](https://arxiv.org/abs/1207.1158v2) and online update at <http://www.slac.stanford.edu/xorg/hfag/>.
 - [7] B. Aubert *et al.* (BaBar collaboration), Phys. Rev. Lett. **98**, 211802 (2007).
 - [8] M. Starič *et al.* (Belle collaboration), Phys. Rev. Lett. **98**, 211803 (2007).
 - [9] T. Aaltonen *et al.* (CDF collaboration), Phys. Rev. Lett. **100**, 121802 (2008).
 - [10] S. Bianco, F. Fabbri, D. Benson, and I. Bigi, Riv. Nuovo Cimento **26N7**, 1 (2003).
 - [11] A. F. Falk, Y. Grossman, Z. Ligeti, Y. Nir, and A. A. Petrov, Phys. Rev. D **69**, 114021 (2004).
 - [12] E. Golowich, J. Hewett, S. Pakvasa, and A. A. Petrov, Phys. Rev. D **79**, 114030 (2009).
 - [13] S. Kurokawa and E. Kikutani, Nucl. Instrum. Meth. Phys. Res., Sect. A **499**, 1 (2003), and other papers included in this volume; T. Abe *et al.*, Prog. Theor. Exp. Phys. **2013**, 03A001 (2013) and following articles up to **2013** 03A011 (2013).
 - [14] A. Abashian *et al.* (Belle Collaboration), Nucl. Instrum. Meth. Phys. Res., Sect. A **479**, 117 (2002); also see the detector section in J. Brodzicka *et al.*, Prog. Theor. Exp. Phys. **2012**, 04D001 (2012).
 - [15] D. J. Lange, Nucl. Instrum. Meth. Phys. Res., Sect. A **462**, 152 (2001); R. Brun *et al.* GEANT 3.21, CERN Report DD/EE/84-1, 1984.
 - [16] N. L. Johnson, Biometrika **36**, 149 (1949).
 - [17] M. Starič *et al.* (Belle collaboration), [arXiv:1212.3478\[hep-ex\]](https://arxiv.org/abs/1212.3478).
 - [18] R. Aaij *et al.* (LHCb collaboration), Phys. Rev. Lett. **111**, 251801 (2013).
 - [19] L. M. Zhang *et al.* (Belle collaboration), Phys. Rev. Lett. **96**, 151801 (2006).